Applied Catalysis B: Environmental 337 (2023) 123014

Contents lists available at ScienceDirect

Applied Catalysis B: Environmental

journal homepage: www.elsevier.com/locate/apcatb

Promoted oxygen release from copper-ceria interfacial sites for selective hydrogen production

Tao Liu [a,b,1], Chunlei Pei [a,b,c,1], Tingting Yang [a,b], Xianhua Zhang [a,b,d], Rui Liu [a,b,d], Zhi-Jian Zhao [a,b,c,d], Jinlong Gong [a,b,c,*]

[a] School of Chemical Engineering and Technology; Key Laboratory for Green Chemical Technology of Ministry of Education, Tianjin University, Tianjin 300072, China
[b] Collaborative Innovation Center for Chemical Science & Engineering (Tianjin), Tianjin 300072, China
[c] Haihe Laboratory of Sustainable Chemical Transformations, Tianjin 300192, China
[d] Joint School of National University of Singapore and Tianjin University, International Campus of Tianjin University, Binhai New City, Fuzhou 350207, China

ARTICLE INFO

Keywords:
Chemical looping
Interfacial sites
Active oxygen species
Methanol reforming
Hydrogen

ABSTRACT

The modulation of oxygen species is an effective strategy for selective H_2 production with relevant chemical looping processes. This paper describes the promoted oxygen release from CuO-CeO_2 redox catalysts for selective H_2 production in chemical looping oxidative steam reforming of methanol (CL-OSRM). Despite the complete oxidation of methanol from CuO, the excess H_2 production of CL-OSRM with respect to methanol steam reforming (MSR) increases linearly with the amount of active oxygen in CeO_2 induced by the copper-ceria interaction. *In situ* spectroscopic characterizations and mechanistic study demonstrate that copper-ceria interfacial sites induce oxygen release from CeO_2 to facilitate the partial oxidation of methoxy to formate species, which promotes the H_2 production rate. This study provides an instructive strategy for the construction of redox catalysts for selective H_2 production with chemical looping processes.

1. Introduction

Methanol steam reforming (MSR) is an important process for H_2 production due to the relatively low reforming temperature and the convenience for transportation of liquids [1]. However, MSR is limited by the endothermic nature and requires external heat, causing high energy consumption [1,2]. As an alternative technology, the chemical looping scheme offers versatile pathways to achieve efficient auto-thermal methanol reforming [3]. The chemical looping oxidative steam reforming of methanol (CL-OSRM) is a combination of methanol conversion and regeneration stages, including complete oxidation (eq1), partial oxidation (eq2), steam reforming (eq3) and regeneration reactions (eq4), in which steam reforming and partial oxidation are dominant for H_2 production.

Complete oxidation:

$$CH_3OH + 3/xMeO = CO_2 + 2H_2O + 3/xMeO_{1-x} (\Delta H < 0) \quad (1)$$

Partial oxidation:

$$CH_3OH + 1/(1-x)MeO_{1-x} = CO_2 + 2H_2 + 1/(1-x)Me \quad (2)$$

Steam reforming:

$$CH_3OH + H_2O = CO_2 + 3H_2 (\Delta H > 0) \quad (3)$$

Regeneration:

$$Me + 1/2O_2 = MeO \quad (4)$$

where Me and MeO represent metal and metal oxides, respectively. In addition, the heat produced from the complete oxidation stage can be utilized to support the endothermic steam reforming reaction, promoting the exergy efficiency in the CL-OSRM process [4–6].

A key issue of the chemical looping scheme is the advancement of redox catalysts [7]. Copper oxides (CuO_x) are thermodynamically active for methanol conversion and the reduced copper-based catalysts exhibit excellent performance in the methanol reforming [8–11]. However, the oxygen release of CuO or Cu_2O is too drastic for selective H_2 production [3]. It still remains challenging to modulate the activity of oxygen species in balancing C-H activation and selective H_2 production [12–14].

* Corresponding author at: School of Chemical Engineering and Technology; Key Laboratory for Green Chemical Technology of Ministry of Education, Tianjin University, Tianjin 300072, China.
E-mail address: jlgong@tju.edu.cn (J. Gong).
[1] These authors contributed equally to this work.

https://doi.org/10.1016/j.apcatb.2023.123014
Received 19 January 2023; Received in revised form 17 May 2023; Accepted 16 June 2023
Available online 17 June 2023

The construction of oxygen-metal interface is a promising strategy to solve this problem [7,15]. Ceria (CeO_2) is a promising candidate due to its high oxygen storage capacity and fluorite structure. In addition, the vital role of interfacial sites of ceria-supported catalysts in catalysis has been demonstrated in several works [16–21]. Copper ions could be doped into ceria lattice and the dopant induces the formation of oxygen vacancies, which improves the reducibility of metal-ceria interface as well as ceria surface [22,23]. The strong metal-ceria synergy facilitates oxygen release from CeO_2[24–26]. These studies provide a perspective that copper-ceria interfacial sites can be active for methanol activation and CeO_2 can serve as a stable oxygen source. However, the mechanism of oxygen release from the metal-ceria interface is still elusive [24,27].

Herein, this paper proposes an interfacial engineering strategy to modulate the reactivity of oxygen species. CuO-CeO_2/Al_2O_3 is designed as a bi-functional redox catalyst which acts as an oxygen carrier for methanol oxidation as well as a catalyst for steam reforming. The redox catalyst exhibits excellent redox performance that the average H_2 production rate can reach 34.7 umol/(g_{cat}•s) and the average CO selectivity goes down to 0.35% per cycle at 220 °C with a H_2O/CH_3OH ratio of 0.5 in the CL-OSRM process. The copper-ceria interaction promotes the oxygen release from CeO_2 and the potential reaction mechanism of the CL-OSRM process were investigated by in-situ spectroscopic characterizations combined with DFT calculations. This work suggests that the rational modulation of oxygen species mediated by the metal-oxide interface can potentially promote the H_2 production for relevant redox chemistry.

2. Experimental section

2.1. Preparation of redox catalysts

CuO-CeO_2/Al_2O_3 redox catalysts with different Cu loading were prepared by coprecipitation method. Al_2O_3 content was fixed to 15 mol % for all samples, which is utilized as a support. The Cu loading was tuned to 1, 2, 4, 8, 15, 30, 45 wt%, named as xCuCeAl (x = 1, 2, 4, 8, 15, 30, 45). The required amounts of $Cu(NO_3)_2$•3 H_2O (99.0%, J&K Scientific), $Ce(NO_3)_3$•6 H_2O (99.0%, Aladdin biological technology Co., Ltd.) and $Al(NO_3)_3$•9 H_2O (98.0%, Aladdin biological technology Co., Ltd.) were dissolved in 50 mL ultrapure water. NaOH aqueous solution (2 M) was added drop by drop at 65 ℃ until the pH reached 10. The mixture was aged at 65 ℃ for 2 h with stirring. The precipitation obtained was separated, washed thoroughly with water 4 times, and dried at 100 ℃ overnight, followed by calcined in ambient air at 400 ℃ for 4 h.

CuO/Al_2O_3 redox catalysts with x wt% Cu defined as xCuAl (x = 8, 15, 30, 45), CeO_2/Al_2O_3 redox catalysts with Al_2O_3 content fixed to 15 mol% defined as CeAl and CuO-CeO_2 redox catalysts with 30 wt% Cu named as 30CuCe were also prepared by the same process as xCuCeAl.

2.2. Material characterizations

Powder X-ray diffraction (XRD) measurements were performed on the D8-Focus X-ray diffractometer using Bruker Cu Kα radiation to determine the crystalline structure of the redox catalysts. The patterns were collected from 2θ angles of 20–80° with a speed of 8°/min.

Quasi in-situ Powder X-ray diffraction (XRD) measurements were taken on the SmartLab X-ray diffractometer using Cu Kα radiation to investigate the dynamic structure evolution of redox catalysts. The 30CuCeAl sample was placed in an in-situ chamber. The CH_3OH/H_2O vapor (the mole ratio of CH_3OH/H_2O is 2) was introduced by N_2 bubble and then the XRD patterns were collected at 220 ℃.

Induced coupled plasma optical emission spectrometry (ICP-OES, Varian Vista-MPX) was carried out to detect the copper content of different redox catalysts.

The N_2 adsorption-desorption tests were performed on a Micromeritics Tristar 300 analyzer at − 196 ℃. The surface areas of redox catalysts were analyzed by the Brunauer-Emmett-Teller (BET) method.

Visible Raman spectra were recorded to investigate the crystalline structure of the redox catalysts using a Renishaw inVia reflex Raman spectrometer with a 532 nm argon-ion laser beam with ten-second integration time. UV-Raman spectra were examined using the same Raman spectrometer but with a 325 nm argon-ion laser beam.

X-ray photoelectron spectra (XPS) were collected to unveil the chemical environment of calcined and reacted redox catalysts, using a Thermo K-Alpha+ spectrometer equipped with a monochromatic Al Kα radiation source. Samples were tableted in the vacuum glove box and sealed in the vacuum bags to avoid re-oxidation of surface copper species.

Transmission electron microscope (TEM) images and element distribution (EDS-mapping) of the samples were performed to examine the morphology of redox catalysts on a JEM-F200 transmission electron microscope.

The temperature-programmed reduction with H_2 (H_2-TPR) was taken to investigate the redox properties of catalysts in a Micromeritics Autochem II 2920 instrument. The setup consisted of a tubular quartz reactor connected to a thermal conductivity detector (TCD). 80 mg sample was placed in a U-tube. Prior to the H_2-TPR analysis, the catalysts were pretreated at 300 ℃ under an argon (Ar) stream for 1 h. Subsequently, the temperature was cooled down to 50 °C. The H_2-TPR experiments were performed by introducing the 10 vol% H_2/Ar flow at a rate of 30 mL/min. The temperature was ramped from 50° to 900°C at a heating rate of 10 °C/min. The amount of H_2 consumption was calculated by integrating the area according to the TCD signal profiles. Assuming CuO is completely reduced to metallic Cu, the theoretical active oxygen from CeO_2 was calculated [22].

$$O_{CeO2} = H_2(total) - H_2(CuO) \quad (5)$$

where O_{CeO_2} is theoretical active oxygen from CeO_2, $H_2(total)$ is the moles of consumed H_2 calculated by H_2-TPR and $H_2(CuO)$ is the moles of H_2 required for CuO completely reduced to metallic Cu (the copper content was analyzed by ICP-OES).

CH_3OH pulse reactions were also performed on the same apparatus (Micromeritics Autochem II 2920) connected with a Hiden QIC-20 mass spectrometer (MS). Typically, 80 mg sample was pretreated at 300 ℃ for 1 h and then the temperature was cooled to 220 ℃. The pulses of H_2O/CH_3OH vapor (H_2O/CH_3OH=0.5, 0.5 mL/pulse) were injected to the quartz reactor. Finally, the output products (CO_2, H_2, H_2O and CO) were detected by the online mass spectrometry (MS).

The specific copper surface areas of different redox catalysts were measured by N_2O titration on a Micromeritics Autochem II 2920 [8,28]. The experiments were conducted with ~100 mg samples. After pre-redution at 300 ℃ under 10 vol% H_2-Ar flow for 1 h, the temperature was cooled down to 90 °C. Then, the exposure to N_2O stream (99.5%, 20 mL/min) at 90 °C led to the oxidation of surface metallic Cu to Cu_2O. Finally, the gas was switched to 10 vol% H_2-Ar flow again and the temperature was ramped to 350 °C at a heating rate of 10 °C/min. The amount of H_2 consumed was calculated by integrating the area detected by the TCD detector. The specific surface area of metallic copper was then calculated based on the amount of H_2 consumed, assuming that the Cu site density is 1.46×10^{19} copper atoms per m^2[28].

To investigate the surface reaction pathway, in situ Diffuse Reflectance Infrared Fourier Transform Spectroscopy (in situ DRIFTS) was conducted using a Thermo Scientific Nicolet IS50 spectrometer equipped with a Harrick Scientific DRIFTS cell and a mercury-cadmium-telluride (MCT) detector. In the CL-OSRM process, the 30CuCeAl sample was outgassed at 300 ℃ firstly and then the temperature was cooled down to 220 ℃ in an Ar flow. Until the spectrum became stable, a background spectrum was obtained. Herein, a flow of Ar bubbled the methanol aqueous solution (H_2O/CH_3OH=0.5) into the reaction cell. The products and intermediates were continuously monitored by in-situ DRIFTS. In the MSR process, the sample was in situ reduced by H_2 first

and the following steps were similar with the CL-OSRM process.

2.3. Computational details

All spin-polarized DFT calculations were performed with the Vienna ab initio simulation package (VASP) [29]. The projector-augmented wave (PAW) method [30] with cutoff energies of 400 eV and the PBE exchange-correlation functional [31] were used. Additionally, we used the DFT+U approach to correct the strong self-interaction of Ce 4 f electrons, with the value of $U_{eff} = 5.0$ eV [32]. The geometric optimization was performed using the convergence criteria with 10^{-5} eV and 0.05 eV/Å for energy and force minimization, respectively. The climbing image nudged elastic band method (CI-NEB) was used to find the transition state [33]. The Cu(111) was modeled by a five-layer slab 4 × 4 unit cell, with 2 × 2 × 1 Monkhorst-Pack k-points grid. And the Cu/CeO_2 interface model contains 64 Cu atoms, 40 Ce atoms and 80 O atoms, the Brillouin zone of which was sampled with a gamma-centered 1 × 1 × 1 k-points grid. A 15 Å vacuum along the z direction was added to separate from the periodically repeated images. The adsorption energies of CH_xO groups were calculated as

$$\Delta E_{CH_3O} = E_{*CH_3O} + \frac{1}{2}E_{H_2} - (E_* + E_{CH_3OH}) \quad (6)$$

$$\Delta E_{CH_2O} = E_{*CH_2O} + E_{H_2} - (E_* + E_{CH_3OH}) \quad (7)$$

$$\Delta E_{CHO} = E_{*CHO} + \frac{3}{2}E_{H_2} - (E_* + E_{CH_3OH}) \quad (8)$$

where E_{*CH_3O}, E_{*CH_2O} and E_{*CHO} are the energy of CH_3O, CH_2O and CHO groups absorbed on the substrate surface (*), respectively. E_{CH_3OH} and E_{H_2} are the energy of gas phase CH_3OH and H_2 molecules.

The reaction energies and the activation energies of elementary reactions were calculated as

$$\Delta E_r = E_{FS} - E_{IS} \quad (9)$$

$$\Delta E_a = E_{TS} - E_{IS} \quad (10)$$

where E_{IS}, E_{TS} and E_{FS} are the energies of the initial state (IS), transition state (TS) and final state (FS), respectively.

The oxygen vacancy formation energies were calculated as

$$\Delta E_{ov} = E_{defect} + E_{H_2O} - E_{perfect} + E_{H_2} \quad (11)$$

where E_{defect}, and $E_{perfect}$ are the energies of the stoichiometric models and the defected models, respectively. E_{H_2O} is the energy of gas phase H_2O molecule.

2.4. Redox activity evaluation

Redox tests were carried out in a fixed bed loaded with 1.2 g catalysts (20–40 mesh) mixed with 10 mL quartz particles. The bed temperature was heated to 220 ℃ in a 160 mL/min flow of N_2. Once the temperature reached 220 ℃, the methanol aqueous solution (0.08 mL/min) with a H_2O/CH_3OH ratio of 0.5 was pumped into a heated chamber via an HPLC pump (P230, Elite, China). Then, the methanol-steam vapor (H_2O/CH_3OH=0.5, $WHSV_{MeOH}$=44.5 kg*s/mol) was fed into the reactor carried by a 160 mL/min flow of N_2 and the reduction stage lasted for 20 min. After the reduction stage, the reactor was purged at 220 ℃ in a 160 mL/min flow of N_2. In the oxidation stage, the gaseous reactants were switched to a 160 mL/min flow of air and this stage lasted for 10 min. Catalytic tests with different H_2O/CH_3OH ratio or at different temperature were also performed by a similar procedure. The stability test was performed over 30CuCeAl sample for 30 continuous cycles and the time for reduction, oxidation and purging (160 mL/min N_2 flow) was set to 20, 10 and 10 min, respectively. In the MSR process, the sample was first reduced by 20 vol% H_2/N_2 flow (200 mL/min) at 300 ℃ for 1 h and cooled down to 220 ℃ under N_2 flow (160 mL/min). Once the temperature reached 220 ℃, the methanol-steam vapor (H_2O/CH_3OH=0.5, $WHSV_{MeOH}$=44.5 kg*s/mol) was fed into the reactor carried by a 160 mL/min flow of N_2 and the reaction lasted for 40 min.

The primary products (H_2, CO_2 and CO) were monitored by an Agilent 490 Micro gas chromatograph (GC) with thermal conductivity detector (TCD). Methanol conversion (%) and CO selectivity (%) were calculated as follows:

$$X_{CH3OH}(\%) = \frac{f_{(CO_2,out)} + f_{(CO,out)}}{f_{(CH_3OH,in)}} \times 100 \quad (12)$$

$$y_{CO}(\%) = \frac{f_{(CO,out)}}{f_{(H_2,out)} + f_{(CO_2,out)} + f_{(CO,out)}} \times 100 \quad (13)$$

where $f(CO_2, out)$, $f(CO, out)$, $f(CH_3OH, in)$ and $f(H_2, out)$ are the flow rate of CO_2, CO, CH_3OH and H_2, respectively.

The average H_2 production rate (A_{H2}, umol/(g*s)) and the average CO selectivity (A_{CO}, %) were calculated as follows:

$$A_{H2} = \frac{\int_0^t f_{(H2,t)}dt}{t} \quad (14)$$

$$A_{CO} = \frac{\int_0^t y_{(CO,t)}dt}{t} \quad (15)$$

where $f(H_2, out)$, and $y(CO, t)$ represent the H_2 production rate and CO selectivity at time t.

3. Results and discussion

3.1. Redox performance and stability

Redox tests were conducted at 220 °C to evaluate the ability of methanol activation over x wt% CuO-CeO_2/Al_2O_3 (denoted as xCuCeAl, x = 8, 15, 30, 45) and CeO_2/Al_2O_3 (denoted as CeAl) redox catalysts. To further investigate the role of lattice oxygen in the CL-OSRM, a low ratio of steam to methanol (S/C=0.5) is required because in the case of high ratio of steam to methanol, it should be taken into consideration that the excess water is another oxidant [3]. It can be observed that the 30CuCeAl sample displays the best performance with the highest H_2 production rate and the lowest CO selectivity among all redox catalysts (Fig. 1a and b). In comparison with the traditional MSR process, the average H_2 production rate of 30CuCeAl sample increases by 20% and the average CO selectivity comes down by 75% per cycle (0–20 min) at 220 °C with a H_2O/CH_3OH ratio (S/C) of 0.5 in the CL-OSRM process (Fig. 1c). Specifically, a higher H_2 production rate can be obtained in the CL-OSRM process (after 5 min), indicating that the active oxygen is consumed for intensified methanol reforming.

To reveal the role of ceria in the CL-OSRM process, the redox experiments of ceria-free 30CuO/Al_2O_3 (denoted as 30CuAl) in the CL-OSRM and MSR processes were performed as reference. In contrast to 30CuCeAl sample, the H_2 production rate over 30CuAl sample in the whole CL-OSRM process is not higher than that of the MSR process (Fig. S3a). In comparison with 30CuAl sample, the addition of ceria (30CuCeAl) promotes the average H_2 production rate and decreases the CO selectivity in one cycle (Fig. S4). Moreover, the H_2O/CH_3OH (S/C=0.5) pulse experiments detected by on-line mass spectra (MS) were performed over 30CuCeAl and 30CuAl samples, providing a perspective of complete oxidation, partial oxidation and steam reforming stages. Due to the participation of H_2O and lattice oxygen, the CL-OSRM is a combination of steam reforming and chemical looping process. It is difficult to exactly distinguish these three stages, because once metallic Cu appears, the catalytic steam reforming starts. In this case, complete oxidation stage mainly includes complete oxidation (eq1) and steam reforming (eq3) reactions; partial oxidation stage is the combination of partial oxidation (eq2) and steam reforming (eq3) reactions; steam

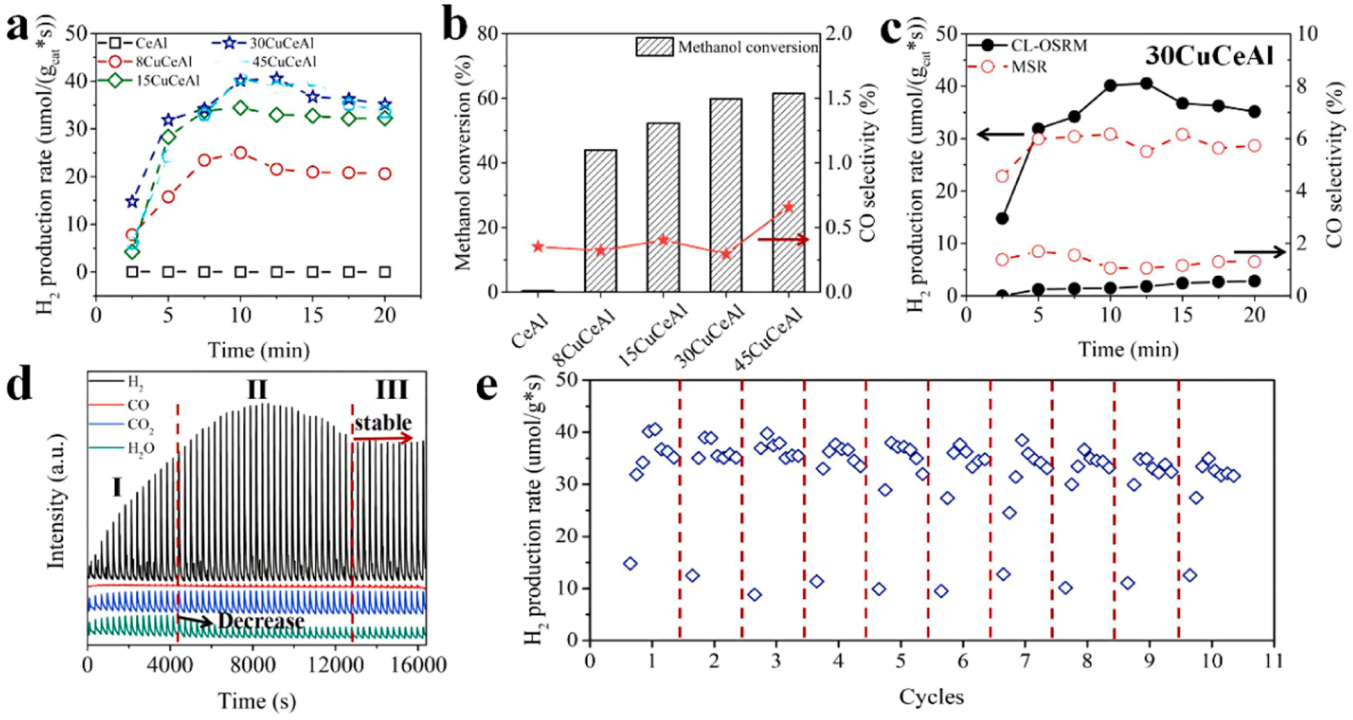

Fig. 1. Redox performance and stability. (a) H_2 production rate of CeAl and xCuCeAl (x = 8, 15, 30, 45) redox catalysts as a function of time in the CL-OSRM process (220 °C, S/C=0.5, $WHSV_{MeOH}$= 44.5 kg*s/mol). (b) The transient methanol conversion and CO selectivity (measured at 10 min) of CeAl and xCuCeAl (x = 8, 15, 30, 45) in the CL-OSRM process (220 °C, S/C=0.5, $WHSV_{MeOH}$= 44.5 kg*s/mol). (c) Redox performance examined on 30CuCeAl in the CL-OSRM (black line) and MSR (red line) processes (220 °C, S/C=0.5, $WHSV_{MeOH}$= 44.5 kg*s/mol). (d) Mass spectral signals for CH_3OH/H_2O pulse tested on 30CuCeAl as a function of time under reaction condition, where stage I , II , III respectively represent complete oxidation, partial oxidation and steam reforming stage. (e) H_2 production rate (0–20 min) over 30CuCeAl in the CL-OSRM process during 10 cycles (220 °C, S/C=0.5, $WHSV_{MeOH}$=44.5 kg*s/mol).

reforming stage dominantly involves steam reforming (eq3) reaction. Hence, we refer the decrease of H_2O signal as the end of complete oxidation stage and the smooth of H_2 signal as the end of partial oxidation stage. For 30CuCeAl sample, the MS signal of H_2 presents an approximate volcano trend which increases first, then decreases and finally becomes stable, undergoing complete oxidation, partial oxidation and steam reforming stages (Fig. 1d). However, for ceria-free 30CuAl sample, the MS signal of H_2 shows different trend which increases first and then becomes stable, mainly undergoing complete oxidation and steam reforming stages (Fig. S3b). These results indicate ceria oxygen species may primarily participate in the partial oxidation of methanol.

CL-OSRM stability test over 30CuCeAl redox catalyst was carried out for 30 consecutive cycles. The transient methanol conversion measured at 10 min maintains relatively stable during 30 cycles, indicating the reversible oxygen release and storage of 30CuCeAl redox catalyst (Fig. S6c). The XRD (Fig. S6d) and TEM (Fig. S6a and b) images demonstrate that the crystallite size (Table S1) and morphology of the 30CuCeAl sample exhibit no obvious changes before and after the 30-cycle reaction. EDS-mapping images of fresh (Fig. S7a) and used 30CuCeAl samples (Fig. S7b) show that the used sample still maintains the uniform elemental distribution. Furthermore, a detailed analysis of the consecutive H_2 stream (0–20 min) during 10 cycles reveals that redox activities of regenerated 30CuCeAl redox catalysts follows the same trend (Fig. 1e), in which the H_2 production rate increases first, then decreases and finally becomes stable. This observation indicates the excellent redox stability of the 30CuCeAl catalyst.

3.2. Copper-ceria interaction activates ceria oxygen species

In order to analyze the promotional role of ceria in redox performance, textural properties of redox catalysts were investigated by microscopic and spectroscopic characterizations. TEM images present that CuO particles with a d spacing of 0.234 nm specified as (111) facet (JCPDS Card No. 48–1548) as well as CeO_2 particles with a d spacing of 0.311 nm and 0.272 nm, specified as (111) facet and (200) facet respectively (JCPDS Card No. 34–0394), are supported on amorphous Al_2O_3 (Fig. 2a). Moreover, the (111) facet of CuO and (111) facet of CeO_2 terminate at the interface, highlighted by the red line. According to XRD profiles of xCCA (x = 0, 8, 15,30, 45) redox catalysts, the typical peaks of CuO and fluorite structure of CeO_2 are found in high copper-loading samples (Fig. 2b). Another observation to be noted is that no compounds like $CuAl_2O_4$ exist in these samples, suggesting weak interactions between copper and aluminum oxides. In comparison with aluminum-free 30CuCe sample, the crystallite sizes of CuO and CeO_2 decrease by the addition of Al_2O_3 (30CuCeAl), indicating that CuO and CeO_2 are well dispersed on the Al_2O_3 (Fig. S8 and Table S1).

To discuss the interaction between the copper and cerium oxides, the crystal structure and symmetry evolution of CeO_2 as the key issue should be considered. Dispersed copper oxides are suggested to be doped into the defective sites on the surface or in the bulk of CeO_2[34]. XRD patterns show a slight shift of the cubic CeO_2(111) diffraction peak toward lower 2θ values in copper-containing samples compared to copper-free samples (Fig. 2c). This shift indicates the incorporation of a small amount of copper ions into the ceria framework. Raman spectra provide additional experimental evidence supporting this incorporation model. The peak in the range of 450–463 cm^{-1}, corresponding to the typical $F_{2\,g}$ band of the fluorite phase [22,35,36], shifts sharply toward lower value from copper-free to copper-contained redox catalysts (Fig. 2d). Furthermore, among copper-contained (x = 8, 15, 30, 45) redox catalysts, the peak shift remains similar, and there is no obvious peak around 590 cm^{-1} dominated by defect-induced mode (D) [37,38]. Therefore, these results suggest that only a small amount of copper ions are doped into ceria lattice, which is corresponding to the results of XRD patterns.

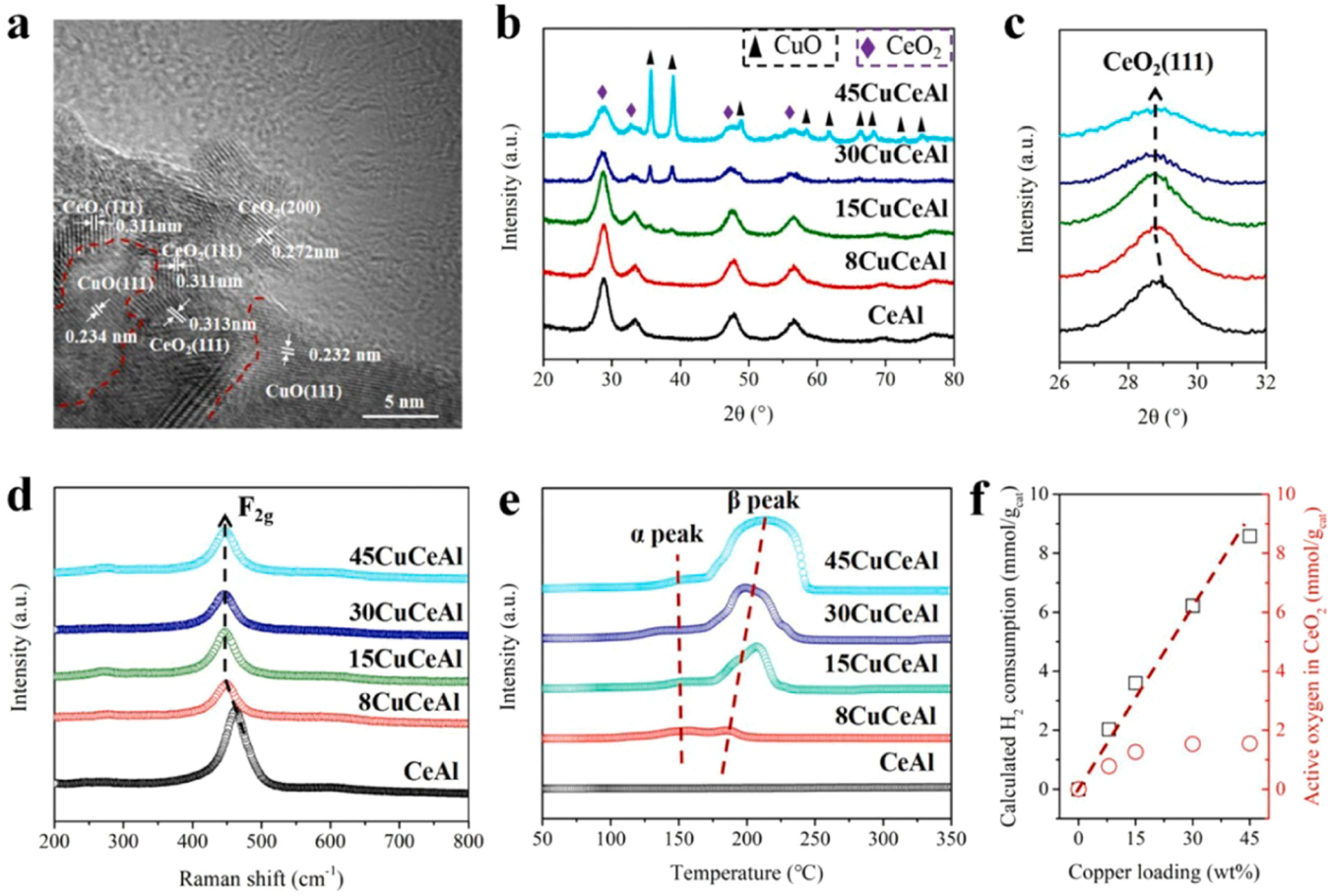

Fig. 2. Morphology and structural characterizations. (a) HR-TEM of fresh 30CuCeAl redox catalyst. (b) XRD patterns and (c) slow sweep of CeAl and xCuCeAl (x = 8, 15, 30, 45) redox catalysts. (d) Visible Raman spectra excited by 532-nm laser line and (e) H_2-TPR of CeAl and xCuCeAl (x = 8, 15, 30, 45) redox catalysts. (f) Calculated H_2 consumption (mmol/g_{cat}) and active oxygen in CeO_2 (mmol/g_{cat}) acquired from H_2-TPR results.

In order to make clear the amount of doping copper ions, the XRD and visible Raman tests of the low copper-loading xCuCeAl redox catalysts (x = 1, 2, 4) were carried out. The shift in the diffraction ray of CeO_2(111) as well as $F_{2\,g}$ mode does not progress as the Cu content increases to 1 wt% (Figs. S9 and S11). It indicates that the incorporation of Cu ions into the CeO_2 crystal lattice becomes saturated at relatively low copper loading, consistent with previous studies [34].

H_2-TPR was conducted to investigate the redox properties of fresh redox catalysts and quantify the amount of active oxygen species in CeO_2. All samples display a dual-mode peak. The peak in the range of 120–300 °C, called α peak, is ascribed to the reduction of small CuO clusters in close contact with CeO_2 (Fig. 2e) and the high-temperature peak around 210 °C, called β peak, is ascribed to the reduction of large CuO particles less interacted with CeO_2[39–41] as well as cerium species at interfacial sites [18,42]. The H_2-TPR results of 30CuCeAl, 30CuAl and CeAl samples (Fig. S12) demonstrate that the copper-ceria interaction induces the CeO_2, especially the interface and surface, to be reduced at a much lower temperature than pure CeO_2. Furthermore, the integral amount of consumed H_2 was calculated by the H_2-TPR patterns for the quantification of active oxygen in CeO_2 [22]. The moles of consumed H_2 are higher than the stoichiometric amounts in CuO for all redox catalysts (Table S2), suggesting that it is not only CuO but also a part of CeO_2 supports are reduced within the range of 120–300 °C. Assuming that copper oxides are completely reduced (ignoring the traceable doping copper ions for high copper-loading redox catalysts), the excessive reduced oxygen atoms from the catalyst are defined as the active oxygen in CeO_2, which is calculated and presented in the Table S2. It can be observed that the active oxygen in CeO_2 grows gradually with the increase of Cu content from 0% to 30% and becomes stable when the Cu content is 30% (Fig. 2f and Table S2). It seems that the active oxygen in CeO_2 achieves a high level when the Cu content comes to 30%. These results suggest that the relative inert oxygen species in CeO_2 can be activated by the synergy between copper and ceria.

3.3. *Activated ceria oxygen species promote methanol partial oxidation*

Quasi in-situ XRD measurements under CH_3OH/H_2O vapor for 30CuCeAl were taken to investigate the dynamic structure evolution of CuO_x-CeO_2 (x ≤ 1). It can be observed that typical diffraction peaks of CuO are observed in the fresh sample, which gradually decrease and disappear after a CH_3OH/H_2O flow feeding in (Fig. 3a). At 1 min, the peaks corresponding to Cu_2O emerge and vanish after 5 min. Then, the new phase of metallic Cu forms and the peak intensity sharpens with continuous exposure to CH_3OH/H_2O vapor (Fig. 3a). In addition, the ex-situ XRD patterns of fresh and reacted 30CuCeAl samples suggest that the whole reduction process from CuO to metallic Cu lasts around 5 min (Fig. S23). Coincidentally, the evolution of H_2/CO_2 mole ratio with reaction time over 30CuCeAl sample (Fig. S14c) has shown that the complete oxidation stage exists within 5 min and then the partial oxidation stage follows, where $H_2/CO_2 < 2$ denotes complete oxidation stage and $2 \leq H_2/CO_2 < 3$ means the partial oxidation stage. Therefore, it is inferred that the lattice oxygen of the copper oxide is active enough to completely oxidize methanol to CO_2 and H_2O. Furthermore, the Cu LMM Auger spectra provided an insight into the surface structure evolution of copper species in the CL-OSRM process. The surface copper species transform from Cu^{2+} (917.5 ev) to a mixture of Cu^{+} (916.0 ev)

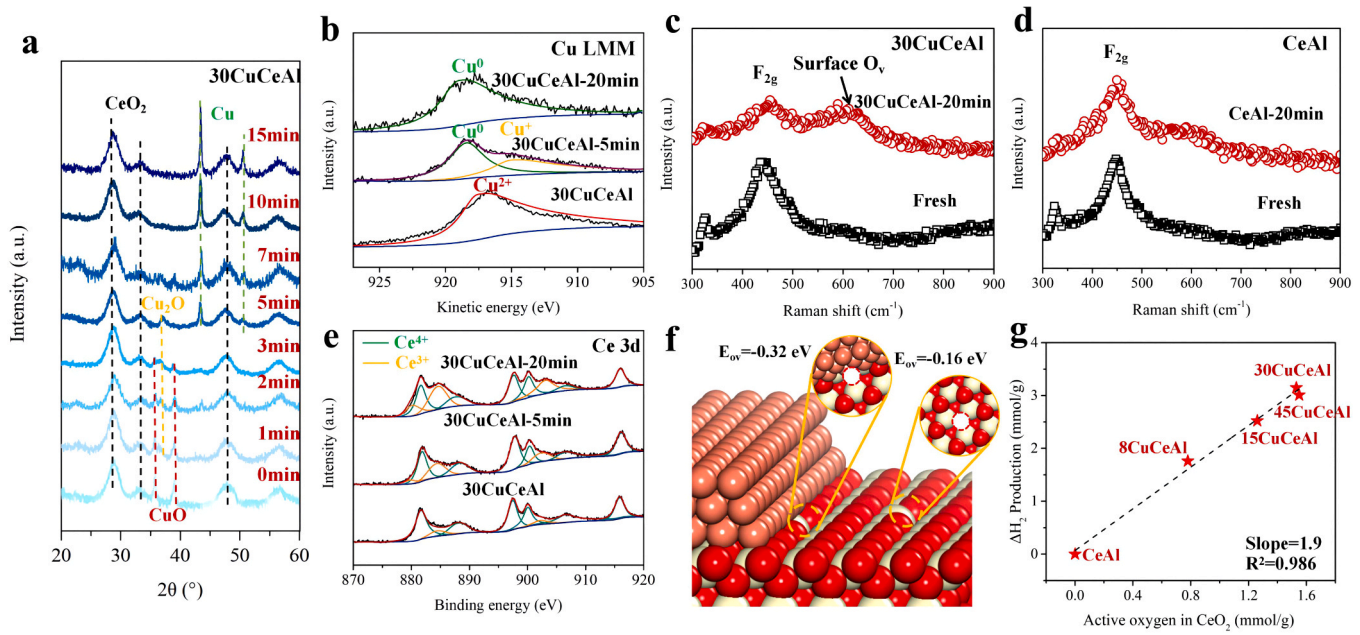

Fig. 3. Copper-ceria interfacial sites for selective H_2 production. (a) Quasi in-situ XRD patterns under CH_3OH/H_2O vapor (bubbled by N_2) over 30CuCeAl catalyst at 220 ℃. The red, yellow, green and black dash lines refer CuO, Cu_2O, Cu and CeO_2, respectively. (b) Auger spectra of Cu LMM regions for the fresh and reacted 30CuCeAl redox catalysts. UV-Raman spectra of fresh (black line) and reacted (red line) (c) 30CuCeAl and (d) CeAl redox catalysts excited by 325-nm laser line. The methanol conversion was taken in one full cycle (20 min). (e) XPS spectra of Ce 3d regions for the fresh and reacted 30CuCeAl redox catalysts. (f) The scheme and formation energy of oxygen vacancies over the Cu/CeO_2 interface and $CeO_2(111)$ surface, where the pink, white and red balls refer Cu, Ce and O atoms, respectively. (g) ΔH_2 value as a function of active oxygen in CeO_2, where ΔH_2 means the accumulative H_2 production detected in the partial oxidation stage of the CL-OSRM process (5–40 min) minus that of the MSR process over xCuCeAl (x = 8, 15, 30, 45) and CeAl redox catalysts.

and Cu^0 (918.4 ev)[8], ultimately becoming dominantly Cu^0 during the reaction (Fig. 3b).

The evolution mechanism of cerium species in CuO_x-CeO_2 under CH_3OH/H_2O flow provides a deep insight into the manner of active oxygen extracted from CeO_2. UV-Raman tests of 30CuCeAl were conducted to investigate the evolution of surface oxygen vacancies in CeO_2 following the introduction of the CH_3OH/H_2O flow. The D mode corresponding to surface O vacancies [34,43] is clearly detected over reacted 30CuCeAl sample after methanol conversion in one cycle, indicating the release of active oxygen from CeO_2 during the reaction (Fig. 3c). To determine whether the oxygen release occurs at the copper-ceria interface or the ceria surface, UV-Raman tests were also performed on copper-free samples (CeAl) under the CH_3OH/H_2O flow for comparison. The D mode assigned to surface oxygen vacancies of ceria at 588 cm^{-1} is not detected [34,43] after the reaction (Fig. 3d). XPS spectra of Ce 3d region provided additional information about near-surface cerium species for calcined and reacted catalysts. The calcined 30CuCeAl initially contained both Ce^{3+} and Ce^{4+} species [17] due to the incorporation of Cu ions into ceria surface and the ratio of Ce^{3+} obviously increases after methanol conversion (Fig. 3e). But no obvious Ce^{3+} peaks were found for reacted CeAl catalysts (Fig. S24). These results exclude the possibility of oxygen removed from CeO_2 surface directly. Furthermore, DFT calculations reveal that the formation energy of oxygen vacancies (short for E_{OV}) over the Cu-CeO_2 interface (−0.32 ev) is lower than that over $CeO_2(111)$ surface (−0.16 ev, Fig. 3 f), suggesting interfacial oxygen species are much easier to be consumed. Based on these results, it can be inferred that the active oxygen species in CeO_2 are consumed from interfacial sites.

To further demonstrate the activity of interfacial sites for partial oxidation over xCuCeAl (x = 8, 15, 30, 45) redox catalysts, the redox activities of xCuAl (x = 8, 15, 30, 45) redox catalysts were evaluated for comparison. The transient H_2 production rate of the xCuCeAl is greater than that of xCuAl despite the similar copper surface areas of the two samples (Fig. S15), indicating that the copper surface is not the sole active site in the partial oxidation stage. Hence, the copper-ceria interface is another possible active site for methanol activation. In addition, the dependence of relative H_2 production on the amount of active oxygen from CeO_2 provides an insight into the role of oxygen release from CeO_2 in selective H_2 production, in which the theoretical active oxygen in CeO_2 is calculated according to the H_2-TPR results (Fig. 2f and Table S2) and the relative H_2 production means the amount of accumulative H_2 production (calculated by the trapezoidal rule according to the Fig. S16) detected in the partial oxidation stage of the CL-OSRM process (5–40 min) minus that of the MSR process over xCuCeAl (x = 8,15,30,45) and CeAl redox catalysts. The relative H_2 production presents a linear correlation with the active oxygen from CeO_2 (Fig. 3 g) and the slope is approximate to 2. As is mentioned from eq2 ($CH_3OH+O^{2-}=CO_2+2\ H_2$), the partial oxidation of methanol is a stoichiometric reaction, where 1 mol oxygen can react with 1 mol methanol to product 2 mol H_2. Hence, it provides quantitative evidence that the consumed oxygen during the partial oxidation stage is dominantly from active oxygen in CeO_2 induced by the copper-ceria interaction. In other words, besides the catalytic reaction over Cu sites, the copper-ceria interface is another active site, which induces active oxygen release from CeO_2 for H_2 production in the partial oxidation stage.

3.4. Reaction mechanism analysis in CL-OSRM

To clarify the mechanism of C-H or O-H breaking over CuO_x-CeO_2 ($x \leq 1$), in-situ DRIFTS experiments of CL-OSRM and MSR processes were performed. The features of methoxy groups (*OCH_3), methyl formate species (CH_3OCH_2O*) and formate species (*CHOO) are detected in the MSR process (Fig. 4a-f), indicating that the MSR reaction follows the methyl formate route (II) (Scheme S1)[8,44,45]. Specifically, the surface methoxy groups sequentially transform to formaldehyde (*OCH_2, difficult to be detected), combine with another *OCH_3 to form methyl formate, then break down to formate and finally decompose to CO_2 and H_2. In this process, the formate species are considered as the key intermediates [46].

Hence, the evolution of the integral peak intensity of formate species

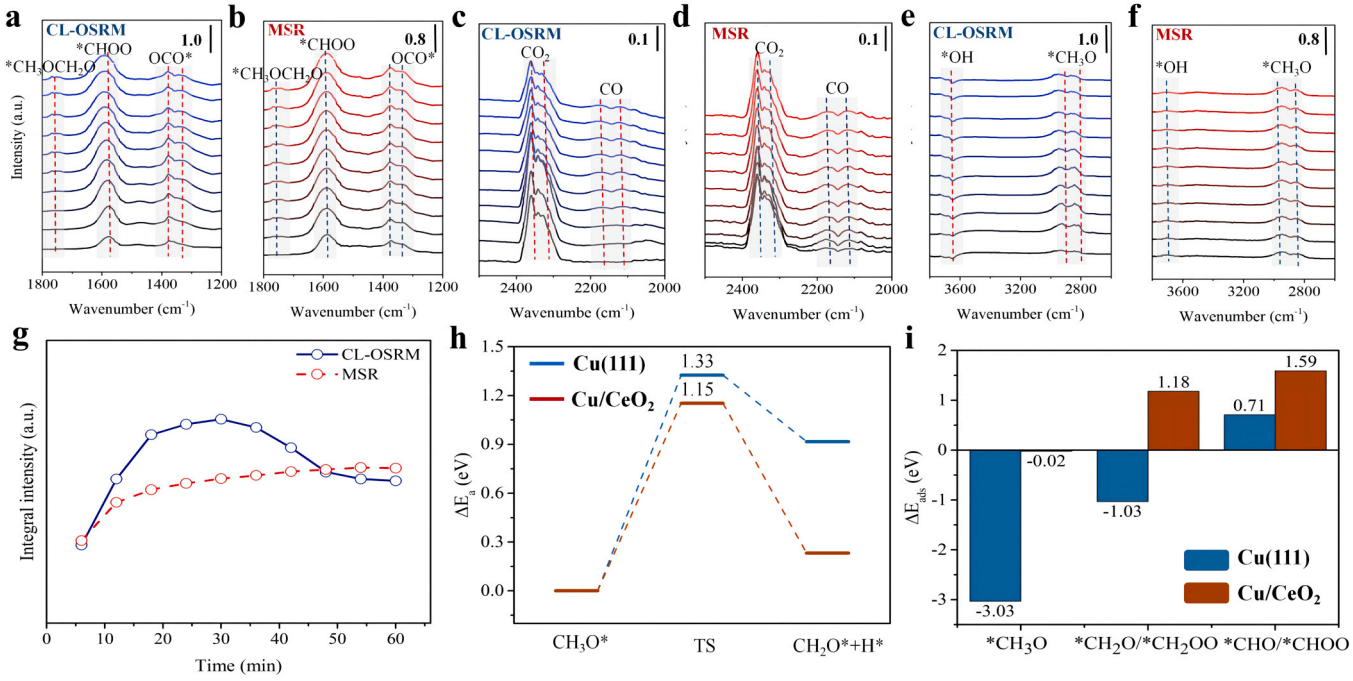

Fig. 4. Surface reaction mechanism of CL-OSRM over CuO_x-CeO_2. In-situ DRIFTS spectra tests on 30CuCeAl in (a)(c)(e) the CL-OSRM process and (b)(d)(f) the MSR process. From bottom to top in each panel: 6, 12, 18, 24, 30, 36, 42, 48, 54, 60 min (g) The integral peak intensity of surface formate species (1600 cm^{-1}) as a function of time in the CL-OSRM and MSR processes. (h) The activation energies of $*CH_3O$ dissociation and (i) the adsorption energies of $*CH_3O$, $*CH_2O$ and *CHO on Cu(111) and Cu/CeO_2 interface, respectively. CH_2OO* and CHOO* present that $*CH_2O$ and *CHO combine the interfacial oxygen to form CH_2OO* and CHOO* -species on the interface.

(key intermediate) at 1600 cm^{-1} provides a deep insight into the reaction mechanism of CL-OSRM process. It can be observed that in the MSR process, the peak intensity increases gradually and maintains at a relatively low level (Fig. 4 g). However, the peak intensity of formate species shows different trend for the CL-OSRM process, which increases sharply for the first 24 min, then decreases from 24 min to 48 min and finally becomes stable (Fig. 4 g). During the complete oxidation stage, methanol is oxidized to H_2O and methoxy groups, following the two-step mechanism [47], and then methoxy groups are further completely oxidized to CO_2 and H_2O, instead of converting to formate species. The sharp increase of formate species indicates that during the partial oxidation stage, the active oxygen species in CeO_2 are induced by the copper-ceria interaction to facilitate the partial oxidation of methoxy groups to formate species, which finally decompose into H_2 and CO_2. Furthermore, the dehydrogenation of methoxy groups to formate species is commonly considered as the rate-determining step of the whole methanol reforming reaction [44,45]. Therefore, the boosting formate species lead to higher H_2 production in the partial oxidation stage.

In addition, the formation of formate species can further influence the CO selectivity in the CL-OSRM process. The peaks of adsorbed CO are weakly detected after 24 min on stream, much later than the MSR process, and with the increase of exposure time, the peak intensity gradually increases from 24 to 60 min (Fig. 4c-d). It has been reported that the methoxy species are likely decomposed to CO [48] while formate species are likely to be decomposed to CO_2[49]. It can be found that the formation of formate species suppresses the generation of carbon monoxide, which illustrates much lower CO selectivity in the CL-OSRM process.

To understand the nature of copper-ceria interfacial sites for H_2 production, DFT calculations provided additional insight into the reaction path of methanol oxidation on the Cu-CeO_2 interface and the Cu (111) facet, respectively. The step of $*CH_3O$ dissociation on Cu(111) is demonstrated as the rate-determining step of methanol oxidation [8]. It is demonstrated that the copper-ceria interface could be the active site that contributes to facilitating the partial oxidation of methoxy groups to formate species, with the activation energy of 1.15 eV (Fig. 4 h), lower than the activation energy of 1.33 eV on Cu(111). By calculating the thermodynamic energy, $*CH_xO$ groups are mainly stabilized at the interfacial sites, that is, the copper-ceria interface could be the active site for continuous dehydrogenation of $*CH_3O$ group (Fig. 4i). Furthermore, the dissociated H is thermodynamically preferred on the O atom of CeO_2(111) surface due to the low reaction energies (Fig. S18), resulting from the BEP relationship [50,51]. Due to the higher activity of interfacial oxygen[52], $*CH_2O$ combines with the interfacial oxygen to form CH_2OO* , and then dehydrogenate to obtain the formate species (Fig. S18), consistent with the results of in-situ DRIFTS (Fig. 4 g). Subsequently, COO* (CO_2) is generated by further dehydrogenation of formate species, and then leaves the interface, resulting in the formation of the interfacial oxygen vacancy, which can be proved by the lower oxygen vacancy formation energy (Fig. 3f) of the metal-support interface than CeO_2(111) surface. DFT calculations demonstrate that copper-ceria interface drives the dehydrogenation of methoxy group to formate species.

On the basis of above discussion, CuO_x surface is considered as the active phase for methanol complete oxidation. Copper-ceria interfacial sites are active for partial oxidation of methanol and the active oxygen in CeO_2 releases fromcopper-ceria interface for selective H_2 production. Upon copper oxides are reduced to metallic Cu, steam reforming takes place on the metallic copper surface. In essence, the copper surface is primarily responsible for catalytic H_2 production in steam reforming, while the copper-ceria interface plays a key role in stoichiometric H_2 production during the partial oxidation stage. The potential reaction paths and mechanism illustration for the CL-OSRM process over CuO-CeO_2/Al_2O_3 are presented in Scheme S1.

4. Conclusions

Chemical looping oxidative steam reforming of methanol (CL-OSRM) is an energy-efficient route for low-temperature H_2 production. CuO-CeO_2/Al_2O_3 is designed as a bi-functional redox catalyst for low-

temperature CL-OSRM. The lattice oxygen from copper oxides is responsible for methanol complete oxidation. In contrast, the active oxygen in CeO_2, induced by the copper-ceria interaction, plays a crucial role in the selective H_2 production during the partial oxidation stage. The amount of active oxygen in CeO_2 shows a linear correlation with the relative H_2 production, further highlighting its significance in H_2 production. In-situ spectroscopic characterizations and DFT calculations provided insights into the mechanism of the CL-OSRM process. It has been demonstrated that copper-ceria interfacial sites induce oxygen release from CeO_2 to facilitate the partial oxidation of methoxy to formate species, which promotes the H_2 production rate. Consequently, the average H_2 production rate can reach 34.7 umol/(gcat•s) and the average CO selectivity goes down to 0.35% per cycle at 220 °C with a H_2O/CH_3OH ratio of 0.5 in the CL-OSRM process. This work suggests that the rational modulation of oxygen species, especially at the interfacial sites, can potentially promote the H_2 production for relevant chemical looping processes.

CRediT authorship contribution statement

Jinlong Gong: Conceptualization, Project administration, Writing – original draft, Writing – review & editing. **Tao Liu:** Investigation, Methodology, Visualization, Data curation, Roles/Writing – original draft, Writing – review & editing. **Chunlei Pei:** Writing – review & editing, Supervision. **Tingting Yang:** Data curation, Validation, Writing – review & editing. **Xianhua Zhang:** Writing – review & editing, Supervision. **Rui Liu:** Methodology. **Zhi-Jian Zhao:** Validation, Writing – review & editing.

Declaration of Competing Interest

The authors declare that they have no known competing financial interests or personal relationships that could have appeared to influence the work reported in this paper.

Data availability

Data will be made available on request.

Acknowledgments

We acknowledge the National Key R&D Program of China (2021YFA1501302), the National Science Foundation of China (No. 22121004, U20B6002, 22122808, 22208242), the Haihe Laboratory of Sustainable Chemical Transformations and the Program of Introducing Talents of Discipline to Universities (BP0618007) for financial support. This work is supported by the XPLORER PRIZE.

Appendix A. Supporting information

Supplementary data associated with this article can be found in the online version at doi:10.1016/j.apcatb.2023.123014.

References

[1] D.R. Palo, R.A. Dagle, J.D. Holladay, Methanol steam reforming for hydrogen production, Chem. Rev. 107 (2007) 3992–4021, https://pubs.acs.org/doi/10.1021/cr050198b.
[2] A.M. Ranjekar, G.D. Yadav, Steam reforming of methanol for hydrogen production: A critical analysis of catalysis, processes, and scope, Ind. Eng. Chem. Res. 60 (2021) 89–113, https://pubs.acs.org/doi/10.1021/acs.iecr.0c05041.
[3] Z. Sun, X. Zhang, H. Li, T. Liu, S. Sang, S. Chen, L. Duan, L. Zeng, W. Xiang, J. Gong, Chemical looping oxidative steam reforming of methanol: A new pathway for autothermal conversion, Appl. Catal. B-Environ. 269 (2020), 118758, https://doi.org/10.1016/j.apcatb.2020.118758.
[4] X. Zhu, Q. Imtiaz, F. Donat, C.R. Muller, F.X. Li, Chemical looping beyond combustion - A perspective, Energy Environ. Sci. 13 (2020) 772–804, https://doi.org/10.1039/C9EE03793D.
[5] X. Zhao, H. Zhou, V.S. Sikarwar, M. Zhao, A.-H.A. Park, P.S. Fennell, L. Shen, L.-S. Fan, Biomass-based chemical looping technologies: The good, the bad and the future, Energy Environ. Sci. 10 (2017) 1885–1910, https://doi.org/10.1039/C6EE03718F.
[6] S.C. Bayham, A. Tong, M. Kathe, L.S. Fan, Chemical looping technology for energy and chemical production, WIRES, Energy Environ. 5 (2016) 216–241, https://doi.org/10.1002/wene.173.
[7] L. Zeng, Z. Cheng, J.A. Fan, L.-S. Fan, J. Gong, Metal oxide redox chemistry for chemical looping processes, Nat. Rev. Chem. 2 (2018) 349–364, https://doi.org/10.1038/s41570-018-0046-2.
[8] D. Li, F. Xu, X. Tang, S. Dai, T. Pu, X. Liu, P. Tian, F. Xuan, Z. Xu, I.E. Wachs, M. Zhu, Induced activation of the commercial $Cu/ZnO/Al_2O_3$ catalyst for the steam reforming of methanol, Nat. Catal. 5 (2022) 99–108, https://doi.org/10.1038/s41929-021-00729-4.
[9] H. Xi, X. Hou, Y. Liu, S. Qing, Z. Gao, Cu-Al spinel oxide as an efficient catalyst for methanol steam reforming, Angew. Chem. Int. Ed. 53 (2014) 11886–11889, https://doi.org/10.1002/anie.201405213.
[10] S. Sa, H. Silva, L. Brandao, J.M. Sousa, A. Mendes, Catalysts for methanol steam reforming - A review, Appl. Catal. B-Environ. 99 (2010) 43–57, https://doi.org/10.1016/j.apcatb.2010.06.015.
[11] K.M. Yu, W. Tong, A. West, K. Cheung, T. Li, G. Smith, Y. Guo, S.C. Tsang, Non-syngas direct steam reforming of methanol to hydrogen and carbon dioxide at low temperature, Nat. Commun. 3 (2012) 1230, https://doi.org/10.1038/ncomms2242.
[12] X. Zhang, C. Pei, X. Chang, S. Chen, R. Liu, Z.J. Zhao, R. Mu, J. Gong, FeO_6 octahedral distortion activates lattice oxygen in perovskite ferrite for methane partial oxidation coupled with CO_2 splitting, J. Am. Chem. Soc. 142 (2020) 11540–11549, https://doi.org/10.1021/jacs.0c04643.
[13] X. Xia, W. Chang, S. Cheng, C. Huang, Y. Hu, W. Xu, L. Zhang, B. Jiang, Z. Sun, Y. Zhu, X. Wang, Oxygen activity tuning via FeO_6 octahedral tilting in perovskite ferrites for chemical looping dry reforming of methane, ACS Catal. 12 (2022) 7326–7335, https://doi.org/10.1021/acscatal.2c00920.
[14] S. Chen, L. Zeng, H. Tian, X. Li, J. Gong, Enhanced lattice oxygen reactivity over Ni-modified WO_3-based redox catalysts for chemical looping partial oxidation of methane, ACS Catal. 7 (2017) 3548–3559, https://doi.org/10.1021/acscatal.7b00436.
[15] S. Chen, C. Pei, X. Chang, Z.J. Zhao, R. Mu, Y. Xu, J. Gong, Coverage-dependent behaviors of vanadium oxides for chemical looping oxidative dehydrogenation, Angew. Chem. Int. Ed. 59 (2020) 22072–22079, https://doi.org/10.1002/anie.202005968.
[16] M. Cargnello, V.V.T. Doan-Nguyen, T.R. Gordon, R.E. Diaz, E.A. Stach, R.J. Gorte, P. Fornasiero, C.B. Murray, Control of metal nanocrystal size reveals metal-support interface role for ceria catalysts, Science 341 (2013) 771–773, https://doi.org/10.1126/science.1240148.
[17] J. Graciani, K. Mudiyanselage, F. Xu, A.E. Baber, J. Evans, S.D. Senanayake, D. J. Stacchiola, P. Liu, J. Hrbek, J. Fernandez Sanz, J.A. Rodriguez, Highly active copper-ceria and copper-ceria-titania catalysts for methanol synthesis from CO_2, Science 345 (2014) 546–550, https://doi.org/10.1126/science.1253057.
[18] A. Chen, X. Yu, Y. Zhou, S. Miao, Y. Li, S. Kuld, J. Sehested, J. Liu, T. Aoki, S. Hong, M.F. Camellone, S. Fabris, J. Ning, C. Jin, C. Yang, A. Nefedov, C. Wöll, Y. Wang, W. Shen, Structure of the catalytically active copper-ceria interfacial perimeter, Nat. Catal. 2 (2019) 334–341, https://doi.org/10.1038/s41929-019-0226-6.
[19] J. Zhu, Y. Su, J. Chai, V. Muravev, N. Kosinov, E.J.M. Hensen, Mechanism and nature of active sites for methanol synthesis from CO/CO_2 on Cu/CeO_2, ACS Catal. 10 (2020) 11532–11544, https://doi.org/10.1021/acscatal.0c02909.
[20] Y. Li, J. Li, X. Yang, X. Wang, Y. Xu, L. Zhang, Preparation of CeO_2-modified Mg(Al)O-supported Pt-Cu alloy catalysts derived from hydrotalcite-like precursors and their catalytic behavior for direct dehydrogenation of propane, Trans. Tianjin Univ. 25 (2018) 169–184, https://doi.org/10.1007/s12209-018-0156-4.
[21] Z.Y. Liu, D.C. Grinter, P.G. Lustemberg, T.D. Nguyen-Phan, Y.H. Zhou, S. Luo, I. Waluyo, E.J. Crumlin, D.J. Stacchiola, J. Zhou, J. Carrasco, H.F. Busnengo, M. V. Ganduglia-Pirovano, S.D. Senanayake, J.A. Rodriguez, Dry reforming of methane on a highly-active $Ni-CeO_2$ catalyst: Effects of metal-support interactions on C-H bond breaking, Angew. Chem. Int. Ed. 55 (2016) 7455–7459, https://doi.org/10.1002/anie.201602489.
[22] A. Davó-Quiñonero, M. Navlani-García, D. Lozano-Castelló, A. Bueno-López, J. A. Anderson, Role of hydroxyl groups in the preferential oxidation of CO over copper oxide-cerium oxide catalysts, ACS Catal. 6 (2016) 1723–1731, https://doi.org/10.1021/acscatal.5b02741.
[23] A.R. Puigdollers, P. Schlexer, S. Tosoni, G. Pacchioni, Increasing oxide reducibility: The role of metal/oxide interfaces in the formation of oxygen vacancies, ACS Catal. 7 (2017) 6493–6513, https://doi.org/10.1021/acscatal.7b01913. ⟨https://⟩.
[24] G.N. Vayssilov, Y. Lykhach, A. Migani, T. Staudt, G.P. Petrova, N. Tsud, T. Skala, A. Bruix, F. Illas, K.C. Prince, V. Matolin, K.M. Neyman, J. Libuda, Support nanostructure boosts oxygen transfer to catalytically active platinum nanoparticles, Nat. Mater. 10 (2011) 310–315, https://doi.org/10.1038/NMAT2976.
[25] J. Guzman, S. Carrettin, A. Corma, Spectroscopic evidence for the supply of reactive oxygen during CO oxidation catalyzed by gold supported on nanocrystalline CeO_2, J. Am. Chem. Soc. 127 (2005) 3286–3287, https://doi.org/10.1021/ja043752s.
[26] J. Guzman, S. Carrettin, J.C. Fierro-Gonzalez, Y.L. Hao, B.C. Gates, A. Corma, CO oxidation catalyzed by supported gold: Cooperation between gold and nanocrystalline rare-earth supports forms reactive surface superoxide and peroxide species, Angew. Chem. Int. Ed. 44 (2005) 4778–4781, https://doi.org/10.1002/anie.200500659.

[27] X.-m Zhang, P. Tian, W. Tu, Z. Zhang, J. Xu, Y.-F. Han, Tuning the dynamic interfacial structure of copper-ceria catalysts by indium oxide during CO oxidation, ACS Catal. 8 (2018) 5261–5275, https://doi.org/10.1021/acscatal.7b04287.
[28] J. Gong, H. Yue, Y. Zhao, S. Zhao, L. Zhao, J. Lv, S. Wang, X. Ma, Synthesis of ethanol via syngas on Cu/SiO_2 catalysts with balanced Cu^0-Cu^+ sites, J. Am. Chem. Soc. 134 (2012) 13922–13925, https://doi.org/10.1021/ja3034153.
[29] Furthmuller Kresse, Efficient iterative schemes for ab initio total-energy calculations using a plane-wave basis set, Phys. Rev. B, Condens. Matter 54 (1996) 11169–11186, https://doi.org/10.1103/PhysRevB.54.11169.
[30] Blochl, Projector augmented-wave method, Phys. Rev. B, Condens. Matter 50 (1994) 17953–17979, https://doi.org/10.1103/physrevb.50.17953.
[31] Burke Perdew, Ernzerhof, Generalized gradient approximation made simple, Physi. Rev. Lett. 77 (1996) 3865–3868, https://doi.org/10.1103/PhysRevLett.77.3865.
[32] M. Akri, S. Zhao, X. Li, K. Zang, A.F. Lee, M.A. Isaacs, W. Xi, Y. Gangarajula, J. Luo, Y. Ren, Y.-T. Cui, L. Li, Y. Su, X. Pan, W. Wen, Y. Pan, K. Wilson, L. Li, B. Qiao, H. Ishii, Y.-F. Liao, A. Wang, X. Wang, T. Zhang, Atomically dispersed nickel as coke-resistant active sites for methane dry reforming, Nat. Commun. 10 (2019) 5181, https://doi.org/10.1038/s41467-019-12843-w.
[33] G. Henkelman, B.P. Uberuaga, H. Jonsson, A climbing image nudged elastic band method for finding saddle points and minimum energy paths, J. Chem. Phys. 113 (2000) 9901–9904, https://doi.org/10.1063/1.1329672.
[34] W.J. Shan, Z.C. Feng, Z.L. Li, Z. Jing, W.J. Shen, L. Can, Oxidative steam reforming of methanol on $Ce_{0.9}Cu_{0.1}O_Y$ catalysts prepared by deposition-precipitation, coprecipitation, and complexation-combustion methods, J. Catal. 228 (2004) 206–217, https://doi.org/10.1016/j.jcat.2004.07.010.
[35] F. Wang, S. He, H. Chen, B. Wang, L. Zheng, M. Wei, D.G. Evans, X. Duan, Active site dependent reaction mechanism over Ru/CeO_2 catalyst toward CO_2 methanation, J. Am. Chem. Soc. 138 (2016) 6298–6305, https://doi.org/10.1021/jacs.6b02762.
[36] H.F. Li, N. Zhang, P. Chen, M.F. Luo, J.Q. Lu, High surface area Au/CeO_2 catalysts for low temperature formaldehyde oxidation, Appl. Catal. B-Environ. 110 (2011) 279–285, https://doi.org/10.1016/j.apcatb.2011.09.013.
[37] X.P. Fu, L.W. Guo, W.W. Wang, C. Ma, C.J. Jia, K. Wu, R. Si, L.D. Sun, C.H. Yan, Direct Identification of active surface species for the water-gas shift reaction on a gold-ceria catalyst, J. Am. Chem. Soc. 141 (2019) 4613–4623, https://doi.org/10.1021/jacs.8b09306.
[38] F. Vindigni, M. Manzoli, A. Damin, T. Tabakova, A. Zecchina, Surface and inner defects in Au/CeO_2 WGS catalysts: Relation between Raman properties, reactivity and morphology, Chem. -Eur. J. 17 (2011) 4356–4361, https://doi.org/10.1002/chem.201003214.
[39] G. Avgouropoulos, T. Ioannides, H. Matralis, Influence of the preparation method on the performance of CuO-CeO_2 catalysts for the selective oxidation of CO, Appl. Catal. B-Environ. 56 (2005) 87–93, https://doi.org/10.1016/j.apcatb.2004.07.017.
[40] C.R. Jung, J. Han, S.W. Nam, T.H. Lim, S.A. Hong, H.I. Lee, Selective oxidation of CO over CuO-CeO_2 catalyst: Effect of calcination temperature, Catal. Today, 93- 5 (2004) 183–190, https://doi.org/10.1016/j.cattod.2004.06.039.
[41] P.F. Zhu, J. Li, S.F. Zuo, R.X. Zhou, Preferential oxidation properties of CO in excess hydrogen over CuO-CeO_2 catalyst prepared by hydrothermal method, Appl. Surf. Sci. 255 (2008) 2903–2909, https://doi.org/10.1016/j.apsusc.2008.08.033.
[42] W.Z. Yu, W.W. Wang, S.Q. Li, X.P. Fu, X. Wang, K. Wu, R. Si, C. Ma, C.J. Jia, C. H. Yan, Construction of active site in a sintered copper-ceria nanorod catalyst, J. Am. Chem. Soc. 141 (2019) 17548–17557, https://doi.org/10.1021/jacs.9b05419.
[43] T. Taniguchi, T. Watanabe, N. Sugiyama, A.K. Subramani, H. Wagata, N. Matsushita, M. Yoshimura, Identifying defects in ceria-based nanocrystals by UV resonance Raman spectroscopy, J. Phys. Chem. C. 113 (2009) 19789–19793, https://doi.org/10.1021/jp9049457.
[44] B.A. Peppley, J.C. Amphlett, L.M. Kearns, R.F. Mann, Methanol-steam reforming on Cu/ZnO/Al_2O_3 catalysts. Part 2. A comprehensive kinetic model, Appl. Catal. A-Gen. 179 (1999) 31–49, https://doi.org/10.1016/S0926-860X(98)00299-3.
[45] B. Frank, F.C. Jentoft, H. Soerijanto, J. Krohnert, R. Schlogl, R. Schomacker, Steam reforming of methanol over copper-containing catalysts: Influence of support material on microkinetics, J. Catal. 246 (2007) 177–192, https://doi.org/10.1016/j.jcat.2006.11.031.
[46] P. Hirunsit, K. Faungnawakij, Cu-Cr, Cu-Mn, and Cu-Fe Spinel-oxide-type catalysts for reforming of oxygenated hydrocarbons, J. Phys. Chem. C. 117 (2013) 23757–23765, https://doi.org/10.1021/jp407717c.
[47] K.-Y. Lee, Y.-J. Huang, Low CO generation on tunable oxygen vacancies of non-precious metallic Cu/ZnO catalysts for partial oxidation of methanol reaction, Appl. Catal. B-Environ. 150 (2014) 506–514, https://doi.org/10.1016/j.apcatb.2013.12.044.
[48] Y. Yu, H. Lei, L. Wang, M. Zhang, Mechanisms of transforming CHx to CO on Ni (111) surface by density functional theory, Trans. Tianjin Univ. 25 (2019) 330–339, https://doi.org/10.1007/s12209-019-00192-0.
[49] H. Li, H. Tian, S. Chen, Z. Sun, T. Liu, R. Liu, S. Assabumrungrat, J. Saupsor, R. Mu, C. Pei, J. Gong, Sorption enhanced steam reforming of methanol for high-purity hydrogen production over Cu-MgO/Al_2O_3 bifunctional catalysts, Appl. Catal. B-Environ. 276 (2020), 119052, https://doi.org/10.1016/j.apcatb.2020.119052.
[50] A. Michaelides, Z.P. Liu, C.J. Zhang, A. Alavi, D.A. King, P. Hu, Identification of general linear relationships between activation energies and enthalpy changes for dissociation reactions at surfaces, J. Am. Chem. Soc. 125 (2003) 3704–3705, https://doi.org/10.1021/ja027366r.
[51] S. Zha, Z.-J. Zhao, S. Chen, S. Liu, T. Liu, F. Studt, J. Gong, Predicting the catalytic activity of surface oxidation reactions by ionization energies, CCS Chem. 2 (2020) 262–270, https://doi.org/10.31635/ccschem.020.201900096.
[52] S. Aranifard, S.C. Ammal, A. Heyden, On the importance of metal-oxide interface sites for the water-gas shift reaction over Pt/CeO_2 catalysts, J. Catal. 309 (2014) 314–324, https://doi.org/10.1016/j.jcat.2013.10.012.